Clim Dyn (2016) 47:433–449
DOI 10.1007/s00382-015-2846-0

Shallowness of tropical low clouds as a predictor of climate models' response to warming

Florent Brient[1] · Tapio Schneider[1,2] · Zhihong Tan[1,2] · Sandrine Bony[3] · Xin Qu[4] · Alex Hall[4]

Received: 11 March 2015 / Accepted: 19 September 2015 / Published online: 5 October 2015

Abstract How tropical low clouds change with climate remains the dominant source of uncertainty in global warming projections. An analysis of an ensemble of CMIP5 climate models reveals that a significant part of the spread in the models' climate sensitivity can be accounted by differences in the climatological shallowness of tropical low clouds in weak-subsidence regimes: models with shallower low clouds in weak-subsidence regimes tend to have a higher climate sensitivity than models with deeper low clouds. The dynamical mechanisms responsible for the model differences are analyzed. Competing effects of parameterized boundary-layer turbulence and shallow convection are found to be essential. Boundary-layer turbulence and shallow convection are typically represented by distinct parameterization schemes in current models—parameterization schemes that often produce opposing effects on low clouds. Convective drying of the boundary layer tends to deepen low clouds and reduce the cloud fraction at the lowest levels; turbulent moistening tends to make low clouds more shallow but affects the low-cloud fraction less. The relative importance different models assign to these opposing mechanisms contributes to the spread of the climatological shallowness of low clouds and thus to the spread of low-cloud changes under global warming.

Keywords Low-clouds · Climate sensitivity · Tropics · Convection · Turbulence

✉ Florent Brient
florent.brient@erdw.ethz.ch

[1] Department of Earth Sciences, ETH Zurich, Zurich, Switzerland

[2] California Institute of Technology, Pasadena, CA, USA

[3] Laboratoire de Météorologie Dynamique (LMD/IPSL), Université Pierre et Marie Curie, CNRS, Paris, France

[4] Department of Atmospheric and Oceanic Sciences, University of California, PO Box 951565, Los Angeles, CA 90095-1565, USA

1 Introduction

For four decades, climate models have exhibited a wide range of equilibrium climate sensitivities, the equilibrium surface temperature increase resulting from doubling of atmospheric CO_2 concentrations (Charney et al. 1979; Bony et al. 2013). The uncertainty in climate sensitivity estimated from different generations of climate models is dominated by uncertainties about how tropical low clouds respond to global warming (Cess et al. 1990, 1996; Bony and Dufresne 2005; Webb et al. 2006; Dufresne and Bony 2008; Vial et al. 2013).

The difficulty of reducing the spread of low-cloud responses to global warming simulated by climate models stems in part from the large variety of processes that control cloudiness, from the microphysics of droplet formation to large-scale dynamics. Several mechanisms for different low-cloud responses have been proposed. For example, an increase of cloudiness under global warming may arise because clear-sky radiative cooling strengthens, destabilizing the planetary boundary-layer (PBL) and increasing the frequency of shallow cumulus convection (Wyant et al. 2009). Conversely, a decrease of cloudiness may arise because the PBL may dry relatively as it deepens (Rieck et al. 2012; Webb and Lock 2013), and convective mixing between the PBL and the drier free troposphere may strengthen (Brient and Bony 2013; Sherwood et al. 2014). Changes of free-tropospheric characteristics associated

with changes in large-scale dynamics (e.g., decreasing relative humidity, weakening subsidence) may also affect low-cloud cover. Several of these mechanisms may simultaneously contribute to low-cloud changes in a warming climate, as demonstrated by Bretherton et al. (2013) using large-eddy simulations.

Dynamical processes controlling low-cloud cover include boundary-layer turbulence and penetrative convection, which lie along a spectrum of turbulent motions that ranges from local eddies with short vertical correlation lengths to non-local plumes with longer vertical correlation lengths. Although part of a continuous spectrum, boundary-layer turbulence and convection are typically represented by distinct parameterization schemes in current climate models and can therefore be analyzed separately. Using single-column models (SCMs), Zhang et al. (2013) show that positive low-cloud feedbacks (reduced low-cloud cover with increasing temperature) arise when the PBL drying induced by enhanced convective moisture transport out of the PBL and/or PBL-top entrainment predominates in the cloud response. Conversely, negative low-cloud feedbacks (increased low-cloud cover) arise when PBL moistening induced by enhanced turbulent moisture transport from the surface upward predominates. Both processes can act simultaneously, and their relative strength controls the sign and intensity of low-cloud feedbacks in models. Indeed, the strength of low-cloud feedbacks in individual climate models can be changed substantially by manipulating either convection schemes (e.g., Gettelman et al. 2012; Tomassini et al. 2014) or turbulence schemes (Watanabe et al. 2012). A broader examination of the effects of parameterized boundary-layer turbulence and convection across climate models would clearly be helpful to understand low-cloud changes.

Here we examine differences in how low clouds are maintained and how they respond to global warming in a set of climate models participating in Phase 5 of the Coupled Model Intercomparison Project (CMIP5, Taylor et al. 2012). Following an overview of the climate models and methods used in this study (Sect. 2), we analyze tropical low-cloud responses to global warming simulated by the models (Sect. 3). We focus on the vertical distribution of tropical low clouds in both the present and future climates, because that turns out to be a good predictor of the low-cloud response. A process-oriented analysis of physical tendencies and sub-grid fluxes using atmosphere-only models (Sect. 4) and a single-column model (Sect. 5) allows us to explain the origin of the spread of tropical low-cloud responses to warming in a subset of the CMIP5 models. Finally, we summarize the results and discuss their implications for constraining the strength of low-cloud feedbacks (Sect. 6).

2 Models and methods

We focus our analyses on the CMIP5 abrupt4xCO2 simulations. They are initialized from the steady state of preindustrial control (piControl) simulations, with atmospheric CO_2 concentrations instantaneously quadrupled from their preindustrial level (280 ppm) and thereafter held fixed. We analyze the warmer climate (10-year average) obtained 130 years after initialization. Additionally, we analyze selected Atmospheric Model Intercomparison Project (AMIP) simulations run with the same models, in which sea surface temperatures (SSTs) are prescribed, and compare them with simulations (AMIP+4K) in which SST are uniformly increased by 4 K.

We analyze changes of cloud radiative effects (CRE) over tropical oceans 30°S–30°N for 21 CMIP5 models (Table 1), with CRE defined as the difference between total and clear-sky radiative fluxes at the top of the atmosphere. Descriptions of boundary-layer, shallow convection, and cloud schemes used in the models are listed in Table 2. Although CRE changes cannot directly be interpreted as an estimate of cloud feedbacks, the spread in CRE changes is a good indicator of the spread of cloud feedbacks (Soden et al. 2004; Bony et al. 2006). In climate change simulations in which CO_2 concentrations are increased, clouds are influenced both by direct radiative effects of CO_2 and by the resulting surface temperature increase (Gregory and Webb 2008). Our interest is primarily in the component associated with SST changes. Because the time-scale of radiative adjustments in response to elevated CO_2 is of order of tens of days (Kamae and Watanabe 2013), focusing on the climate change after the first year of the abrupt4xCO2 simulations isolates the slower component of CRE changes associated with SST changes. Therefore, we compute CRE changes (ΔCRE) and corresponding SST changes (ΔSST) as differences between years 131–140 and years 2–6 of the abrupt4xCO2 simulations.[1] From the monthly-mean CRE and SST changes, we compute the sensitivity of CRE changes relative to SST changes in bins of monthly-mean vertical velocity ω at 500 hPa (with 5 hPa/day bins), following Bony et al. (2004) and Bony and Dufresne (2005), as

$$\Sigma_\omega = \frac{\Delta \mathrm{CRE}_\omega}{\Delta \mathrm{SST}_\omega}. \quad (1)$$

Integrating over all dynamical regimes (identified by vertical velocity ω) and weighting by their frequency of occurrence P_ω (the probability density function of ω) gives the total CRE sensitivity

[1] Averaging over a longer time period (e.g., years 2–11 after initialization) does not impact our results.

Table 1 Equilibrium climate sensitivity (ECS, K), shallowness index (γ, %), tropical mean CRE changes ΔCRE (W m^{-2}), SST changes (K), and corresponding CRE sensitivities Σ (W m^{-2} K^{-1}) for 21 CMIP5 models

	Model acronym	ECS	piControl	abrupt4xCO2			AMIP+4K
			γ	ΔCRE	ΔSST	Σ	Σ_a
1	GISS-E2-R	2.1	19 ± 2	−0.97	0.98	−1.06	
2	BNU-ESM	4.1	48 ± 2	−1.63	1.98	−0.93	
3	GISS-E2-H	2.3	18 ± 2	−0.91	1.26	−0.84	
4	MIROC5*	2.7	38 ± 2	−0.95	1.35	−0.70	−0.11
5	GFDL-ESM2G	2.4	38 ± 4	−0.39	1.08	−0.67	
6	GFDL-ESM2M	2.4	39 ± 3	−0.54	1.45	−0.49	
7	CCSM4	2.9	49 ± 3	−0.84	1.89	−0.39	−0.80
8	inmcm4	2.1	89 ± 1	−0.29	1.09	−0.30	
9	NorESM1-M	2.8	47 ± 3	−0.36	1.56	−0.19	
10	bcc-csm1-1	2.8	47 ± 2	−0.06	1.19	−0.09	−0.33
11	MRI-CGCM3*	2.6	35 ± 4	0.13	1.73	−0.05	0.35
12	bcc-csm1-1-m	2.9	49 ± 3	0.36	1.99	0.15	
13	CanESM2	3.7	74 ± 3	1.09	2.34	0.40	0.25
14	IPSL-CM5B-LR	2.6	83 ± 2	0.63	1.76	0.43	0.35
15	MPI-ESM-LR*	3.6	70 ± 4	1.33	2.43	0.59	0.77
16	MPI-ESM-MR	3.4	72 ± 4	1.32	2.29	0.62	0.72
17	HadGEM2-ES*	4.6	4 ± 3	1.66	2.59	0.69	0.42
18	GFDL-CM3	4.0	44 ± 4	2.34	2.28	1.10	
19	MIROC-ESM	4.7	74 ± 2	3.95	3.03	1.47	
20	IPSL-CM5A-MR	4.1	70 ± 4	4.43	3.28	1.53	
21	IPSL-CM5A-LR*	4.1	70 ± 5	4.51	3.05	1.75	1.23
	Multi-model mean	3.2 ± 0.8	53 ± 20	0.7 ± 1.8	1.9 ± 0.7	0.1 ± 0.8	0.3 ± 0.6

ECS values are listed in Forster et al. (2013) and Sherwood et al. (2014). Shallowness indices γ are mean values plus/minus one standard deviation estimated from temporal variations in weak-subsidence regimes in the piControl simulations. The CRE and SST changes in the abrupt4xCO2 simulations are differences between years 131–140 and 2–6. The Σ_a column shows the CRE sensitivity obtained from fixed SST simulations, comparing simulations with global SST increased by 4 K (AMIP+4K) to control (AMIP) simulations. Models are numbered in order of increasing Σ for the abrupt4xCO2 simulations. AMIP models with asterisks provide the physical tendencies used in Sect. 4

$$\Sigma = \int_{\omega} P_{\omega} \Sigma_{\omega} \, d\omega. \tag{2}$$

Computing the total CRE sensitivity in this way gives results that are statistically indistinguishable from computing a total CRE sensitivity as the ratio of total CRE to SST changes, ΔCRE/ΔSST (Table 1); however, the two ways of computing the total CRE sensitivity are not identical but are related by the geometric-arithmetic mean inequality. CRE sensitivities for specific dynamical regimes can be similarly computed by restricting the integral in (2) to vertical velocities characterizing a dynamical regime.

By our analysis period 130 years after the beginning of the abrupt4xCO2 simulations, the models exhibit a large spread of tropical SST changes of ΔSST = 1.9 ± 0.7 K (uncertainties are given as 1 standard error), with a range across models between 1.0 and 3.3 K (Table 1). This SST change is strongly correlated with the models' equilibrium climate sensitivity ($R = 0.90$) reported by Forster et al. (2013). The spread in CRE sensitivity is likewise large, $\Sigma = 0.1 \pm 0.8$ W m^{-2} K^{-1}, with values ranging from −1.1 to +1.8 W m^{-2} K^{-1}, similar to the range seen in CMIP3 models (Bony and Dufresne 2005). The CRE sensitivity is strongly correlated with the tropical SST change ($R = 0.87$) and, by implication, with the equilibrium climate sensitivity ($R = 0.74$). The CRE sensitivity Σ is also strongly correlated with the CRE sensitivity of atmosphere-only simulations in which SST is uniformly increased by 4 K ($R = 0.85$ using the 10 models for which the needed output is available, Table 1).

In what follows, we identify models by numbers, assigned in order of increasing CRE sensitivity Σ from abrupt4xCO2 simulations. We separate models into low-sensitivity (LS) and high-sensitivity (HS) groups according to their CRE sensitivities and separated by the sign of Σ, with 10 and 11 models in the two groups, respectively.

Most of the spread in Σ among models is contributed by the different CRE sensitivities Σ_{ω} in weak-subsidence

Table 2 Principal parameterization schemes for low clouds used in CMIP5 models

	Model acronym	PBL schemes	Shallow convection schemes	Cloud schemes
1,3	GISS-E2	Moeng and Sullivan (1994)	Genio and Yao (1993), Genio et al. (1996)	Sundqvist et al. (1989)
2	BNU-ESM	Neale et al. (2010)	Zhang and McFarlane (1995), Hack (1994)	Slingo (1987)
4	MIROC5	Mellor and Yamada (1974), Mellor and Yamada (1982), Watanabe et al. (2010)	Chikira and Sugiyama (2010), Pan and Randall (1998)	Watanabe et al. (2009)
5,6	GFDL-ESM2	Anderson et al. (2004)	Moorthi and Suarez (1992)	Tiedtke (1993), Anderson et al. (2004)
7	CCSM4	Neale et al. (2010)	Zhang and McFarlane (1995), Hack (1994)	Slingo (1987)
8	inmcm4	Blackadar (1962)	Betts (1986)	Volodin and Dianskii (2004)
9	NorESM1-M	Neale et al. (2010)	Zhang and McFarlane (1995), Hack (1994)	Slingo (1987)
10,12	bcc-csm1	Neale et al. (2010)	Zhang and Mu (2005), Wu et al. (2010)	Slingo (1987)
11	MRI-CGCM3	Mellor and Yamada (1974), Mellor and Yamada (1982)	Yukimoto et al. (2011)	Tiedtke (1993)
13	CanESM2	McFarlane et al. (1992)	Salzen et al. (2005)	von Salzen et al. (2013)
14	IPSL-CM5B	Yamada (1983)	Hourdin et al. (2013)	Jam et al. (2013), Bony and Emanuel (2001)
15,16	MPI-ESM	Brinkop and Roeckner (1995), Louis (1979)	Tiedtke (1989), Stevens et al. (2013)	Sundqvist et al. (1989)
17	HadGEM2-ES	Lock et al. (2000)	Gregory and Rowntree (1990)	Smith (1990)
18	GFDL-CM3	Anderson et al. (2004)	Bretherton et al. (2004)	Tiedtke (1993), Donner et al. (2011)
19	MIROC-ESM	Mellor and Yamada (1974), Mellor and Yamada (1982)	Arakawa and Schubert (1974), Emori et al. (2001)	Treut and Li (1991)
20/21	IPSL-CM5A	Louis (1979), Laval et al. (1981)	Emanuel (1991), Emanuel (1993)	Bony and Emanuel (2001)

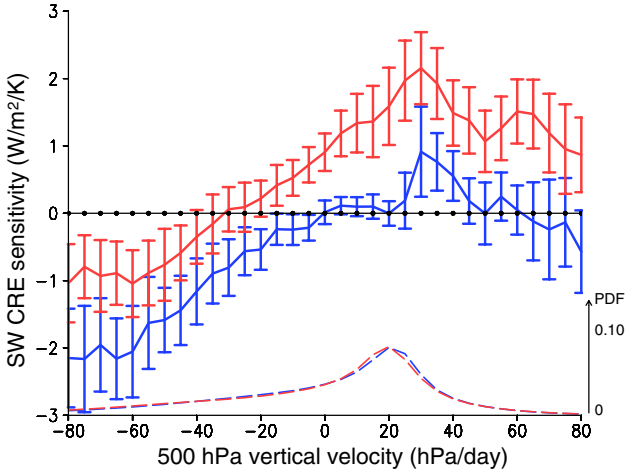

Fig. 1 SW component of CRE sensitivities Σ_ω for high (*red*) and low (*blue*) sensitivity models, for different dynamical regimes identified by their monthly-mean 500-hPa vertical velocity ω. Here and in subsequent figures, the changes in the abrupt4xCO2 simulations are differences between years 131–140 and years 2–6. *Solid lines* indicate multi-model means, and *error bars* plus minus one intermodel standard deviation for each group. Probability density functions P_ω of ω are represented as *dashed lines*

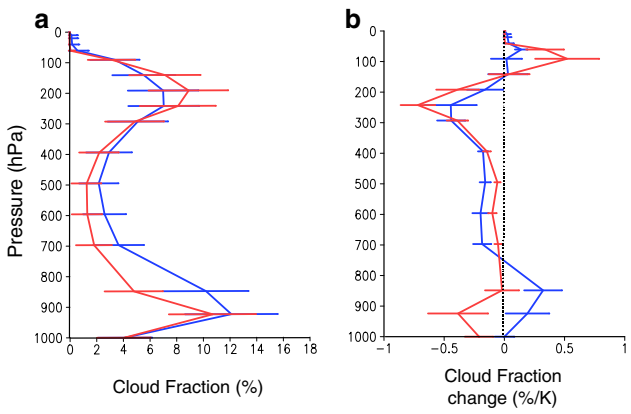

Fig. 2 Vertical distribution of cloud fraction in pre-industrial control climate (**a**) and changes induced by surface warming in abrupt4xCO2 simulations (**b**) in weak-subsidence regimes over tropical oceans ($\omega_{500} = 20 \pm 10$ hPa day^{-1}). The *lines* show averages over models with higher (*red*) and lower (*blue*) CRE sensitivity Σ. The *horizontal bars* indicate plus minus one intermodel standard deviation for each group. Each monthly-mean cloud fraction over model-dependent vertical levels was linearly interpolated to the 17 standard CMIP5 layers to facilitate comparison of the different models

regimes, especially through the shortwave component of CRE (Fig. 1). Therefore, we focus our analyses on weak-subsidence regimes, identified by vertical velocities $\omega = 20 \pm 10\,\mathrm{hPa\,day^{-1}}$. Vertical velocities in this band occur frequently over tropical oceans (P_ω is maximum at $\omega \approx 20\,\mathrm{hPa\,day^{-1}}$). The coarse partitioning into HS and LS models and the focus on weak-subsidence regimes allows us to identify fundamental model differences that contribute to the spread of CRE sensitivities.

3 Vertical distribution of tropical low clouds

3.1 Differences between HS and LS climate models

In weak-subsidence regimes, models with higher and lower CRE sensitivity differ in the vertical distribution of cloud fractions they simulate in the pre-industrial control climate (Fig. 2a), and they differ in the response of this vertical distribution to global warming (Fig. 2b). HS models generally simulate a lower minimum of cloud fraction in the middle and lower troposphere than LS models, especially between 700 and 900 hPa; cloud fractions in the upper troposphere in HS models tend to be slightly larger than in LS models. The vertical distribution of clouds suggests that on average, HS models tend to have a shallower PBL than LS models, consistent with an average stronger lower-tropospheric static stability (15.3 versus 14.6 K potential temperature difference between 700 and 1000 hPa, respectively).

In response to global warming, the tropopause rises in all models, and clouds above 400 hPa correspondingly shift upward (Fig. 2b). This is expected given the radiative constraints on the height of the tropopause and of deep clouds (e.g., Held 1982; Thuburn and Craig 1997; Hartmann and Larson 2002; Singh and O'Gorman 2012). HS and LS models mainly differ in their cloud fraction changes below 850 hPa (∼1.4 km altitude): cloud fraction in HS models decreases on average, whereas it increases in LS models.

3.2 Shallowness of low clouds

The average vertical distributions of cloud fractions mask the great variety of vertical distributions simulated by climate models in weak-subsidence regimes. Given the apparent importance of differences in the vertical distribution of lower-tropospheric cloud fractions, we introduce an index

$$\gamma = \frac{\mathrm{CF}_{950}}{(\mathrm{CF}_{850} + \mathrm{CF}_{950})}, \tag{3}$$

which quantifies the ratio of cloud fraction below the 900-hPa level (∼1 km), CF_{950}, to the total low-cloud fraction below the 800-hPa level (∼2 km), $\mathrm{CF}_{850} + \mathrm{CF}_{950}$. The cloud fractions CF_{950} and CF_{850} are the mass-weighted cloud fractions between 1000 and 900 hPa and between 900 and 800 hPa, respectively. These values are calculated from the cloud fractions on model vertical levels (rather than the standard CMIP5 levels). The shallowness index γ quantifies the fraction of low clouds below 900 hPa, irrespective of the absolute low-cloud fraction for each model: $\gamma = 100\,\%$ indicates that low clouds are present only below 900 hPa and the above-lying layer between 800 and 900 hPa is cloud free; conversely, $\gamma = 0\,\%$ indicates low clouds are present only in the layer between 800 and 900 hPa and the layer underneath is cloud free. The absolute cloud fraction is normalized out because it influences the amplitude of the low-cloud CRE response to global warming without modifying its sign, through a radiative feedback between cloud radiative effects, temperature and relative humidity (Brient and Bony 2012). It may also be tuned in models to be close to observations. By contrast, the vertical distribution of clouds is a better signature of physical characteristics of boundary-layer and shallow convection parametrizations (e.g., Watanabe et al. 2012; Yao and Cheng 2012). Note that Nuijens et al. (2015) adopted a slight variant of this shallowness index γ to analyze observations.

In weak-subsidence regimes, CMIP5 models produce values of shallowness indices γ between 19 and 89 %, with intermodel variations (average standard deviation of 20 %) larger than the standard deviation from temporal variations (∼3 %, Table 1). This suggests different models assign very different relative importances to the diverse physical processes that influence clouds below 2 km altitude, and that γ is a characteristic of climate models. For comparison, the corresponding shallowness γ obtained from ERA Interim reanalyses (Dee et al. 2011) for the years 1979–2012 is $45 \pm 3\,\%$ (errors indicating one seasonal standard deviation), and that obtained from Calipso/GOCCP (GCM-Oriented CALIPSO Cloud Product) satellite data (Chepfer et al. 2010) for the years 2006–2012 is $44 \pm 3\,\%$. These values lie in the middle of the range of values seen in the CMIP5 models; however, the ERA Interim value may be contaminated by model biases, and the satellite value by cloud overlap and masking effects.

In the CMIP5 models, shallower low clouds (larger γ) are generally associated with stronger surface sensible heat fluxes (SHF) in weak-subsidence regimes (Fig. 3a). The variation of SH fluxes across models is primarily accounted for by variations in the air-sea temperature difference ($R = 0.82$) and secondarily by variations in surface wind speed ($R = 0.32$). Variations across models of the air-sea temperature difference in weak-subsidence regimes, in turn, arise primarily through variations in surface air temperature ($R = -0.73$) and secondarily through variations in SST ($R = -0.43$). That is, models with lower surface air temperature in weak-subsidence regimes tend to have stronger SHF and shallower low clouds. The lower surface

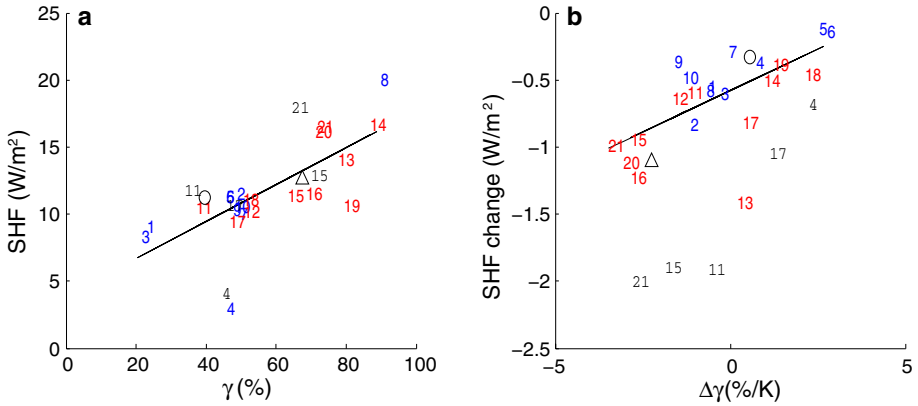

Fig. 3 Relationship between shallowness (γ) of tropical maritime low clouds and sensible heat flux in weak-subsidence regimes over tropical oceans. **a** Pre-industrial climate ($R = 0.77$). **b** Changes induced in abrupt4xCO2 simulations between years 2–6 and 131–140 ($R = 0.64$). Here and in subsequent figures, HS and LS models are marked by *red* and *blue* numbers (cf. Table 1). Also included (*black numbers*) are five models for which AMIP and AMIP+4K configurations are compared (cf. Table 1). Results from the single-column version of the IPSL model are also included for two configurations: one (control simulation) with convective parameterization active (*triangle*) and another with the convective parameterization switched off (*circle*)

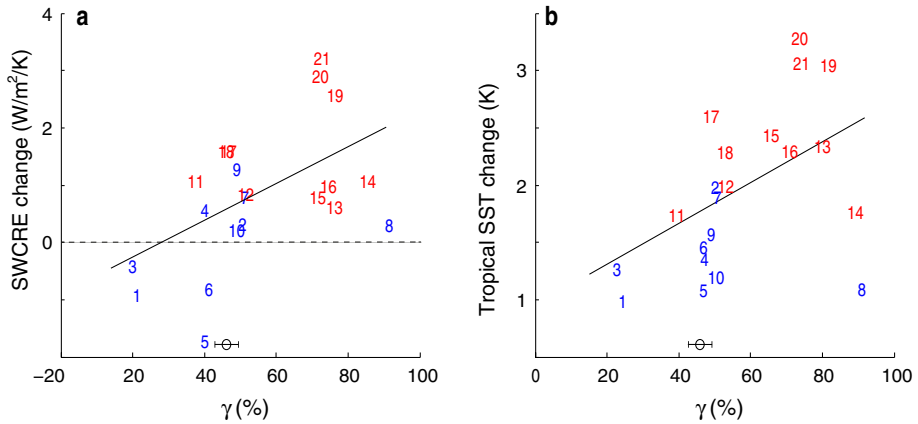

Fig. 4 Relationship between shallowness (γ) of tropical maritime low clouds and **a** changes of shortwave cloud radiative effects and **b** tropical-mean sea surface temperature (**b**) in weak-subsidence regimes over tropical oceans. The shallowness γ is evaluated for the pre-industrial control climate. Changes are those between years 131–140 and 2–6 in the abrupt4xCO2 simulations for SWCRE ($R = 0.53$) and tropical SST ($R = 0.49$). Observational shallowness estimates are represented by a *circle* near the *lower axis*, with *whiskers* indicating one seasonal standard deviation

air temperature may be linked to the shallower vertical distribution of clouds and the atmospheric radiative cooling exerted by them. Figure 3a also confirms that HS models (red numbers) generally simulate shallower low clouds than LS models (blue numbers).

Not only have models with shallower low clouds stronger SH fluxes in weak-subsidence regimes, their response to global warming follows a similar pattern. Sensible heat fluxes generally decrease as the climate warms because the lower atmosphere stabilizes; the decrease in SH fluxes and increase in net radiative energy input to the surface are balanced by an increase in latent heat fluxes. Models with a stronger reduction in SH fluxes under global warming tend to produce deeper low clouds (reduced γ; see Fig. 3b). However, the shallowness of low clouds can increase or decrease under global warming in different models, and changes in γ do not clearly separate HS and LS models.

The relationship between the shallowness of low clouds in weak-subsidence regimes in the pre-industrial control climate and a model's sensitivity of shortwave cloud radiative effects (SWCRE) to SST in experiments when CO_2 concentrations are quadrupled is shown in Fig. 4a. As before, the changes exclude the fast response in the first year of the abrupt4xCO2 simulations. Figure 4a shows that shallower low-clouds are associated with a more positive

shortwave feedback by low clouds. Consistent with the strong correlation between SW cloud feedback and climate sensitivity, Fig. 4b confirms that shallower low clouds in subsidence regimes are generally associated with higher tropical SST changes and hence with higher climate sensitivity. Variations of the climatological shallowness γ account for about half the spread (intermodel standard deviation) of tropical SST changes and climate sensitivities among models. So the shallowness of low clouds is a good predictor of a model's climate sensitivity.

If we assume the low-cloud shallowness inferred from observations and reanalysis (around $\gamma \approx 45 \pm 4\,\%$) is an adequate representation of reality, and models with a similar low-cloud shallowness are closer to being correct than models that farther diverge from the observational value, the results in Fig. 4 suggest that models with extremely high or low γ and climate sensitivity are unlikely to be correct. The least sensitive model that has a shallowness γ within the observed range has a climate sensitivity of 2.4 K (#5, GFDL-ESM2G). The most sensitive model with a shallowness γ within the observed range has a climate sensitivity of 4.6 K (#17, HadGEM2-ES). However, this spread of climate sensitivities is only about 30 % smaller than the total spread among all models.

The sensitivity of global warming to present-day shallowness of low clouds in GCMs raises the question of which physical processes are responsible for the different vertical distributions of low clouds and their changes under global warming.

4 Role of parameterizations in controlling cloud responses

4.1 Turbulence and convection

To identify which parameterization schemes are responsible for the different vertical distributions of low clouds and their changes under global warming, we analyze tendencies associated with different parameterization schemes in AMIP simulations, using AMIP+4K simulations to represent global warming. Only the atmosphere-only CMIP5 simulations provide physical tendencies, and only five models provide every tendency needed (Table 1). These five models span different climate sensitivities and exhibit cloud radiative changes ranging from moderately negative to strongly positive. Their behavior is representative of that seen in the CMIP5 simulations, in terms of present low-cloud shallowness (γ) and changes of it under global warming (Fig. 3). In weak-subsidence regimes, three of the models simulate a deepening of low clouds under warming, and two models simulate a shallowing (Fig. 3b).

Various parameterization schemes affect low-cloud cover in the models (Table 2). Turbulence and convection in the five models are represented by separate schemes, as commonly done, although they are part of a continuous spectrum of convective motions. For example, shallow convective cumulus clouds typically rise above convective plumes that have their roots in a turbulent boundary layer. Yet shallow convection and boundary layer turbulence are typically represented by separate schemes that do not explicitly interact. The tendencies affecting specific humidity and thus low-cloud cover in the models we analyze arise from parameterization schemes for turbulence (specific humidity tendency due to diffusion, CMIP5 variable *tnhusd*), convection (specific humidity tendency due to convection, CMIP5 variable *tnhusc*), and condensation and boundary layer processes (specific humidity tendency due to stratiform clouds/precipitation and boundary-layer mixing, CMIP5 variable *tnhusscpb*).[2] Figure 5 shows the corresponding mean specific humidity tendencies in weak-subsidence regimes at heights below the 700 hPa level. The sum of these specific humidity tendencies represents the total tendency of parameterized processes (CMIP5 variable, *tnhusmp*), which balances tendencies owing to resolved processes such as large-scale subsidence and horizontal advection.

Some aspects of the parameterized tendencies are robust across models. Every model simulates a moistening tendency by the sum of parameterized processes in the boundary layer, which is compensated by large-scale subsidence drying (not shown). The total parameterized tendency arises primarily through turbulent moistening in the boundary layer, which is partially compensated by convective drying. The tendencies owing to parameterized turbulence and convection have opposite sign but are similar in their vertical shapes and magnitudes. Some models simulate significant cloud fraction at the top of PBL (800 hPa), driven by convective (e.g., HadGEM-A) or turbulent (e.g., MPI-ESM) moistening. However, the tendencies owing to parameterized convection differ greatly among the models, both in magnitude and in vertical structure.

Figure 5 also shows the parameterized tendencies in the corresponding AMIP+4K simulations, again with some results that are robust across models. Surface latent heat fluxes and specific humidities increase as the climate warms, resulting in stronger turbulent moistening in the PBL. This is compensated by strengthened subsidence drying, arising because specific humidity gradients across the top of the PBL strengthen—a consequence of the temperature increase

[2] For the MPI-ESM-LR and HadGEM-A models, turbulence and condensation are not separated and are combined in the "turbulence" tendencies.

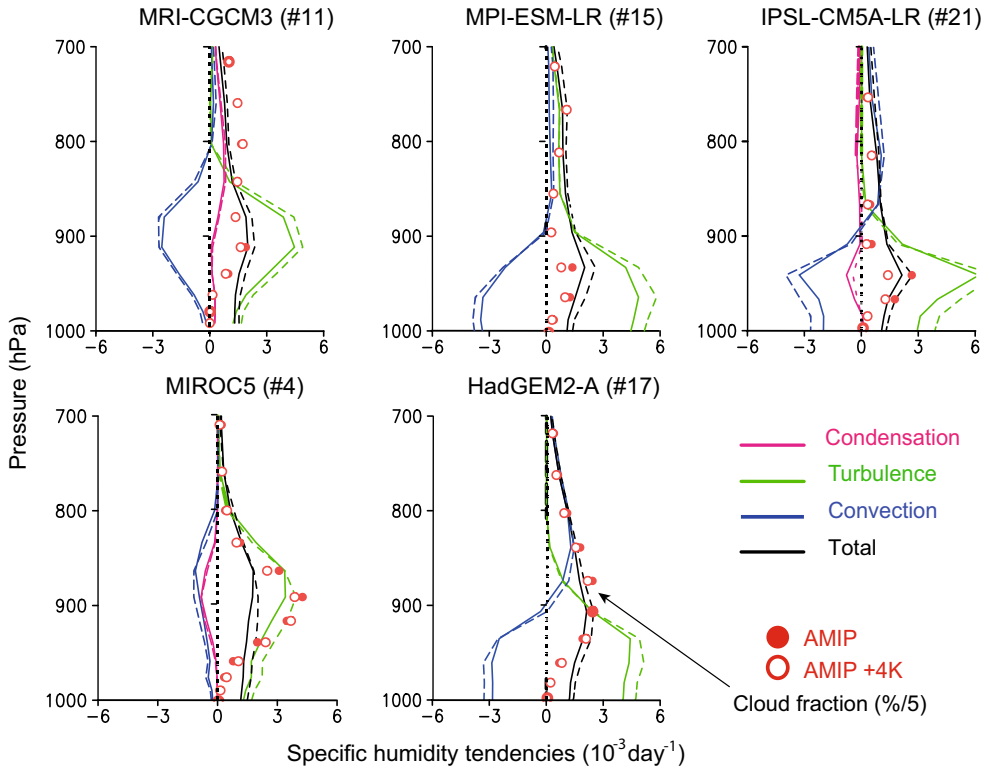

Fig. 5 Specific humidity tendencies in weak-subsidence regimes over tropical oceans for five models simulating deepening (*top*) and shallowing (*bottom*) of low clouds under surface warming. *Filled* and *dashed lines* are AMIP and AMIP+4K simulations, respectively. Tendencies owing to parameterized condensation (*pink*), turbulence (*green*) and convection (*blue*) are shown, as well as the total of parameterized tendencies (*black*). Mean cloud fraction (divided by 5) is shown by *filled* and *empty dots* for AMIP and AMIP+4K simulations

that, by the Clausius–Clapeyron relation, implies strengthened specific humidity gradients when relative humidity changes are comparatively small (Held and Soden 2006; Schneider et al. 2010; Brient and Bony 2013). Because the PBL specific humidity and its vertical gradients increase, convective drying also strengthens (e.g. Sherwood et al. 2014), but to a lesser extent than turbulent moistening. By contrast, parameterized temperature tendencies are less affected by the surface temperature increase, because vertical temperature gradients in the lower atmosphere change less than specific humidity gradients. Thus, the spread of cloud responses in CMIP5 models appears to be more directly related to changes in parameterized specific humidity tendencies and their effect on low clouds than to parameterized temperature tendencies. Similar analyses can be carried out focusing on relative humidity tendencies (Fig. 6); however, changes in relative humidity tendencies can also result from local radiative feedbacks (Brient and Bony 2012).

4.2 Low-cloud inhibition by convective drying

In every model, parameterized convection dries and turbulence moistens the lower troposphere. They add up to a net moistening effect, with different relative strengths among models. Figure 5 shows that the strength of convective drying at the altitude of maximum cloudiness varies greatly among models. We quantify the low-cloud inhibition by convective drying through the index

$$\varepsilon_c = -\frac{\int_{p_s}^{800\,\mathrm{hPa}} H(-Q_c)\, Q_c\, \mathrm{CF}\, dp}{\int_{p_s}^{800\,\mathrm{hPa}} Q_t\, \mathrm{CF}\, dp}, \tag{4}$$

where Q_c is the specific humidity tendency due to convection, Q_t is the total specific humidity tendency due to parameterized processes, H is the Heaviside step function, and CF is the cloud fraction. The greater ε_c, the stronger the drying of cloudy levels by parameterized convection. Figure 7a and Table 3 show that greater values of ε_c are associated with shallower low clouds (greater γ) in weak-subsidence regimes. As the climate warms, models with higher values of ε_c in the present-day climate tend to exhibit a deepening of the low clouds, as indicated by a negative change of γ ($R = -0.95$, Fig. 7b). Identical conclusions arise by computing (4) with relative humidity tendencies, due to high correlation with ε_c ($R = 0.99$, not shown). This suggests that investigating how low-cloud

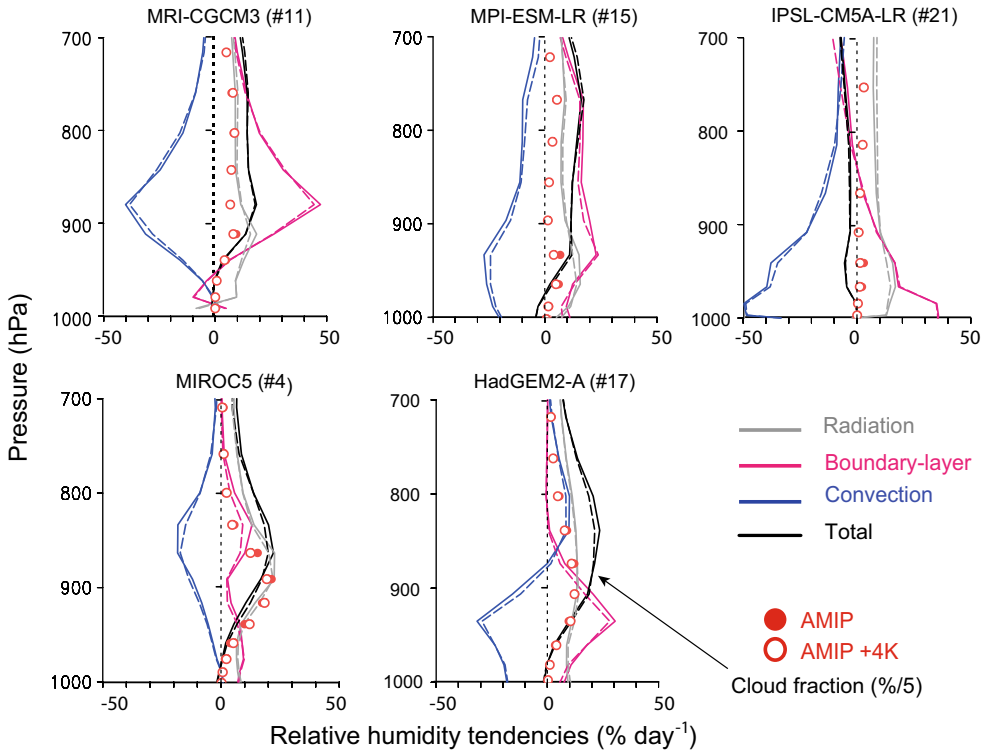

Fig. 6 As Fig. 5 but for relative humidity tendencies. Tendencies (total in *black*) are separated into those associated with parameterized radiation (*grey*), condensation and turbulence in the boundary layer (*pink*), and convection (*blue*)

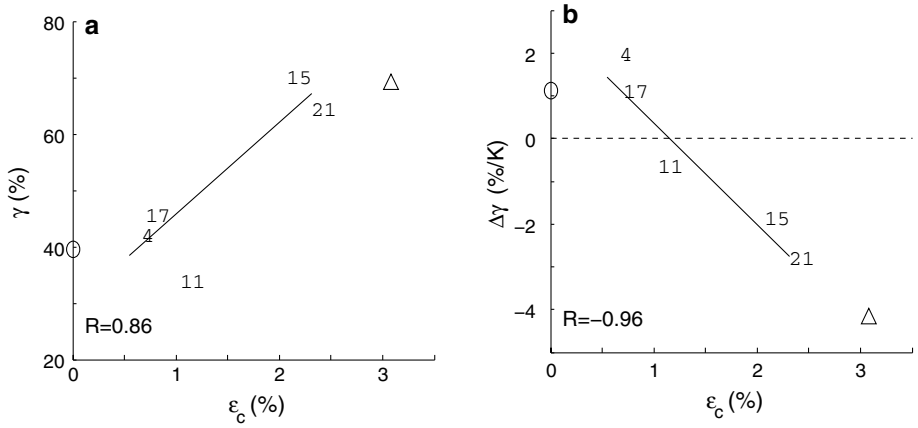

Fig. 7 Relationships between convective drying index (ε_c) and **a** shallowness (γ) of low clouds in weak-subsidence regimes over tropical oceans for AMIP simulations or **b** changes in shallowness ($\Delta\gamma$) between AMIP and AMIP+4K simulations relative to AMIP. The models are identified by numbers (Table 3). Results from the single-column version of the IPSL model are also included for two configurations: one (control simulation) with convective parameterization active (*triangle*) and another with the convective parameterization switched off (*circle*) (however, they are excluded in the calculation of the linear regression lines and correlation coefficients that are also shown)

shallowness is controlled may also help identify causes of low-cloud changes under global warming. However, the deepening as measured by changes in γ may be caused by different changes of cloud fractions at the lowest levels (below 900 hPa) relative to those above (between 800 and 900 hPa). For example, the deepening is caused by a strong decrease of cloud cover below 900 hPa in models #15 and #21, whereas an increase of cloud cover at higher levels also contributes to the deepening in model #11 (see Table 3 for model names). Nevertheless, parameterized

Table 3 Shallowness index (γ), convective drying index (ϵ_c), specific humidity diffusivity (K_{mp}), sensible fluxes, latent heat fluxes, and buoyancy fluxes B computed as SHF + 0.07 LHF. Tropical-ocean average (first lines) and normalised changes (second lines) over weak subsidence are listed for every model. Normalized changes are calculated by the difference between AMIP4K-AMIP for the five atmospheric models, and by the difference under a 2-K warming for the two single-column models

Model acronym		γ (%)	ϵ_c (%)	K_{mp} (m^2 s^{-1})	SHF, LHF, B (W m^{-2})		
MIROC5	4	42	−0.6	8.4	4.1	150	14.6
		2.0	0.00	−0.10	−0.18	5.6	0.21
MRI-CGCM3	11	34	−1.0	8.5	11.8	145	22.0
		−0.6	0.02	0.20	−0.49	6.3	−0.05
MPI-ESM-LR	15	70	−2.1	6.4	12.9	139	22.6
		−1.9	0.05	0.16	−0.50	5.9	−0.10
HadGEM2-ES	17	46	−0.7	8.1	10.7	150	21.2
		1.1	−0.02	−0.18	−0.28	5.2	0.09
IPSL-CM5A-LR	21	65	−2.3	5.8	18.0	135	27.4
		−2.8	0.00	0.28	−0.57	6.4	−0.12
IPSLA SCM		69	−3.1	3.9	12.8	119	21.1
		−4.2	−0.40	0.10	−0.64	3.7	−0.38
IPSLA SCM (no cv)		40	0.0	3.2	11.4	111	19.1
		1.1	0.00	−0.02	−0.17	4.0	0.11

convective drying appears to be an important predictor of both the shallowness of present low clouds and its response to climate change.

4.3 Mixing efficiencies

The results so far indicate that greater shallowness of low clouds in weak-subsidence regimes is associated with greater climate sensitivity of models, stronger sensible heat fluxes, weaker near-surface static stability (i.e., greater air-sea temperature difference), and stronger convective drying. Models with stronger convective drying tend to exhibit a stronger decrease of low clouds at the lowest levels. This suggests that the shallowness of low clouds, and its response to climate change, is related to the efficiency of parameterized moisture mixing in models, similar to what was suggested by Sherwood et al. (2014).

Irrespective of whether the parameterized processes are diffusive, we quantify the moisture mixing efficiency of parameterized processes in the models through an effective diffusivity $K_i(z)$, defined through the relation

$$\left(\frac{d\bar{q}}{dt}\right)_i = -\frac{1}{\bar{\rho}}\frac{\partial}{\partial z}\left(\bar{\rho}\,\overline{w'q'}\right)_i = -\frac{1}{\bar{\rho}}\frac{\partial}{\partial z}\left(-\bar{\rho}K_i\frac{\partial\bar{q}}{\partial z}\right), \tag{5}$$

where ρ is density, q the specific humidity, and $(d\bar{q}/dt)_i$ is its tendency owing to a parameterized process labeled with index i (e.g., boundary-layer turbulence or convection, as shown in Fig. 5). The overbar denotes grid-scale (resolved) variables, and the flux $\overline{w'q'}$ is the density-weighted mean of the parameterized subgrid-scale fluxes, which are, for the purposes of quantifying mixing efficiency, represented diffusively (notwithstanding that this would not be an adequate representation, e.g., for convective fluxes or precipitation). The implied diffusivity $K_i(z)$ can be obtained from the available parameterized tendencies by vertical integration of (5) from the level z to the top of the atmosphere, where $\bar{\rho}(z) \to 0$, giving

$$\begin{aligned}\bar{\rho}(z)\left(\overline{w'q'}\right)_i(z) &= \int_z^\infty \bar{\rho}\left(\frac{d\bar{q}}{dt}\right)_i dz \\ &= -K_i(z)\,\bar{\rho}(z)\left(\frac{\partial\bar{q}(z)}{\partial z}\right).\end{aligned} \tag{6}$$

To determine $K_i(z)$ from the relation (6), we linearly interpolate the specific humidities $\bar{q}$ from the 17 standard CMIP5 levels to the model-specific native levels, on which the tendencies $(d\bar{q}/dt)_i$ are available. We use monthly-mean fields in all analyses, which may blur fine structures such as the sharp inversion at the top of PBL; however, it provides a coarse estimate of the moisture mixing in the lower troposphere. The so determined total diffusivities $K = -\left(\overline{w'q'}\right)_i(z)/\left(\frac{\partial\bar{q}(z)}{\partial z}\right)$ for the sum of all parameterized processes below 2 km are negatively correlated with the shallowness γ ($R = -0.94$), implying that shallower clouds are associated with weaker total mixing.

As the climate warms, changes in the subgrid-scale fluxes $\left(\overline{w'q'}\right)_i$ according to the conceptual diffusive closure (6) can arise because the implied diffusivities K_i change, because specific humidity gradients $\partial\bar{q}/\partial z$ change, or because there are covariances between these two changes:

$$\Delta\left(\overline{w'q'}\right)_i = -\left(\frac{\partial\bar{q}}{\partial z}\right)\Delta K_i - K_i\,\Delta\left(\frac{\partial\bar{q}}{\partial z}\right) - \Delta K_i\,\Delta\left(\frac{\partial\bar{q}}{\partial z}\right) \tag{7}$$

Calculating the implied subgrid-scale fluxes and their changes according to relations (6) and (7), averaging over the lowest 2 km (below 800 hPa) of the atmosphere, and

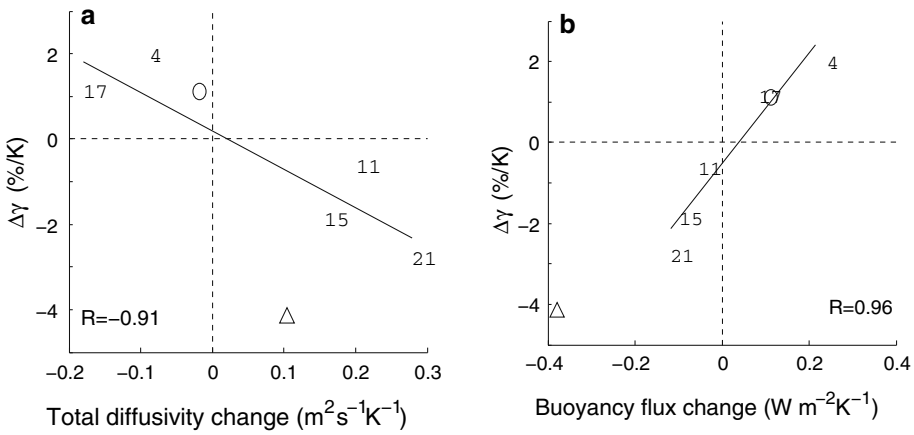

Fig. 8 Relationship between changes in shallowness γ of low clouds in weak-subsidence regimes over tropical oceans and **a** changes in total humidity diffusivity ΔK by all parameterized processes and **b** changes in buoyancy flux computed as $\Delta\text{SHF} + 0.07\Delta\text{LHF}$. *Symbols* as defined in Fig. 7

decomposing the changes according to the right-hand side of (7), we find the following in tropical weak-subsidence regimes:

1. The total vertical specific humidity flux $\overline{w'q'}$ owing to the sum of all parameterized processes strengthens as the climate warms. This is a direct consequence of the strengthened large-scale advective drying in subsidence regimes, confirmed by the increase of net surface evaporation ($E - P > 0$) at the surface (Mitchell et al. 1987; Held and Soden 2006).
2. The specific humidity gradient $\partial\bar{q}/\partial z$ strengthens (becomes more strongly negative), as is to be expected from the Clausius–Clapeyron relation when relative humidities near the surface change little as the climate warms (e.g., Boer 1993; Held and Soden 2006; Schneider et al. 2010).
3. The implied total diffusivity K for the sum of all parameterized processes for some models increases and for others decreases as the climate warms. An increasing diffusivity (stronger mixing) is associated with deepening low clouds (γ decreases), and a decreasing diffusivity is associated with shallowing of low clouds (Fig. 8a).
4. Shallowing low clouds (γ increases) are also associated with increasing surface buoyancy fluxes,[3] and deepening low clouds (γ decreases) with decreasing surface buoyancy fluxes (Fig. 8b). Boundary-layer radiative changes induced by low clouds and mixing may both contribute to the sensible heat flux and buoyancy flux changes under warming in climate models.

[3] Surface buoyancy fluxes B are related to surface fluxes through the relation $B \propto (\text{SHF} + 0.61\,((c_p\bar{T})/L_v)\,\text{LHF})$ where LHF is the surface latent heat flux. In the tropics, the coefficient multiplying LHF is close to 0.07 (Cuijpers and Bechtold 1995). We thus use the approximation $B \propto (\text{SHF} + 0.07\text{LHF})$.

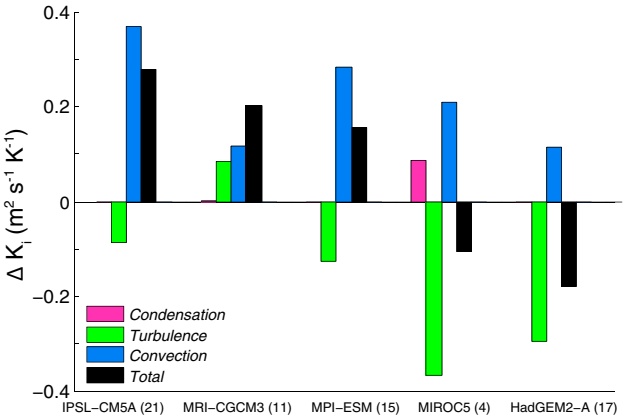

Fig. 9 Changes of retrieved total humidity diffusivity K_i between AMIP+4K and AMIP simulations, averaged from 800 hPa to the surface in weak-subsidence regimes over tropical oceans. Changes of diffusivities associated with all parameterized processes (*black*) are decomposed into condensation (*pink*), turbulence (*green*) and convection (*blue*) terms. The total diffusivity changes decrease from left to right across the models

5. Covariances between changes in diffusivity and changes in specific humidity gradients are small (not shown).

By decomposing the diffusivity changes into components associated with different parameterized processes (Fig. 9), we see that every model simulates weakened turbulent moisture mixing and strengthened convective moisture mixing, with the exception of the MRI model, in which mixing by parameterized turbulence strengthens slightly. The turbulent moisture mixing likely weakens because the sensible heat flux weakens as the climate warms, weakening buoyancy fluxes, and because of the increasing static stability and increasing importance of the buoyancy effects (virtual temperature effects) of water vapor loading (e.g., Pierrehumbert 2002; O'Gorman and Schneider 2008). A strong latent heat flux increase may partially

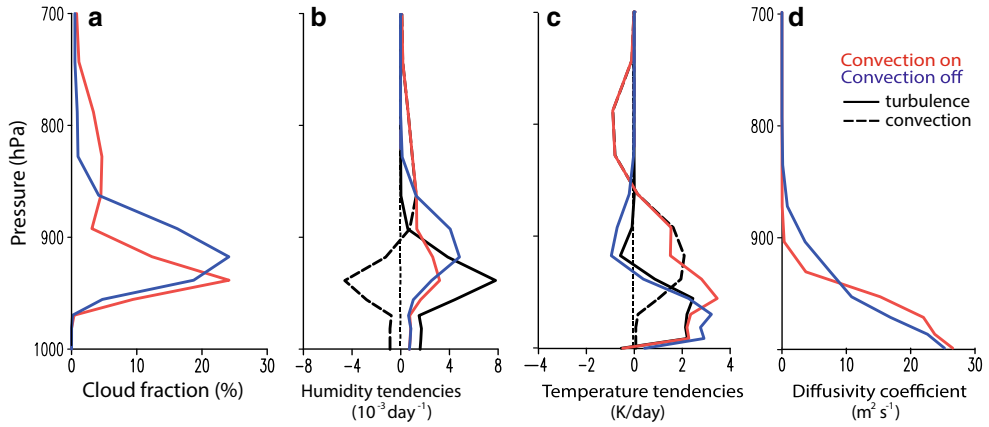

Fig. 10 Cloud fraction and parameterized tendencies in IPSL-CM5A SCM with (*red*) and without (*blue*) convection parameterization. **a** Cloud fraction, **b** specific humidity tendencies, **c** temperature tendencies and **d** turbulent diffusivity from the model turbulence parameterization are represented. Total (turbulent plus convective) tendencies from experiments with convection (*red lines*) are separated into tendencies owing to parameterized turbulence (*black solid lines*) and into tendencies owing to parameterized convection (*black dashed lines*) in **b** and **c**

compensate this effect in the AMIP simulations (Fig. 8b; Table 3), in which the surface energy balance is not energetically closed. Nevertheless, CMIP models also show a wide spread of buoyancy flux changes (from −0.28 to 0.37 W m^{-2} K^{-1}), associated with changes of shallowness (not shown) and mostly related to the spread of sensible heat flux changes (Fig. 3b). The opposing changes in turbulent and convective mixing are consistent with the compensation between convective drying and turbulent moistening seen in the vertical profiles of specific humidity tendencies (Fig. 5). The relative importance in different models of these two robust mixing changes gives rise to the different responses of the vertical distribution of low clouds as the climate warms. To demonstrate this explicitly, we turn to experiments with a single-column version of one model.

5 Testing the role of the convective parameterization in a single-column model

We use a single-column model version of the IPSL-CM5A GCM to perform experiments testing the sensitivity of low clouds to the convection parameterization. While the IPSL GCM, like other models, exhibits biases in its representation of observed tropical low clouds (e.g. Nuijens et al. 2015), the SCM reproduces the cloud fraction of the parent GCM in weak-subsidence regimes (e.g., the S6 case studied by Zhang et al. 2013), provided a stochastic forcing is added to the vertical velocity (Brient and Bony 2013). Each sensitivity experiment is run for 200 days, and results are analyzed after 60 days of spin-up.

Like the parent GCM (Fig. 5), the IPSL-CM5A SCM simulates shallow low clouds (high γ), with a cloud fraction maximum near 950 hPa (Fig. 10a). This is associated with strong turbulent moistening and convective drying in the cloud layer (Fig. 10b). Temperature tendencies show turbulent warming near the surface, overlain by convective warming and turbulent cooling (Fig. 10c). Above about 900 hPa, convection cools and moistens the lower troposphere. The turbulence parameterization in the IPSL-CM5A model uses an exponentially decreasing diffusivity with height (Fig. 10d), typical of stable cloud layers (Louis 1979). Note that the profile of turbulent diffusivity calculated by (6) is identical to the one given by the model seen in Fig. 10d (not shown).Thus, substantial turbulent mixing and, with it, turbulent moistening are confined below about 1 km in this model. The shallowness of the low clouds is a consequence.

If we disable the parameterized convection, the turbulence parameterization compensates for some of the missing convection effects. The turbulent specific humidity tendency below the cloud layer is reduced, compensating for some of the missing convective drying; it is increased around and above 900 hPa, compensating for some of the missing convective moistening (Fig. 10b). However, the total humidity transport increases and has a more elevated maximum, though with more rapid decay with altitude above it. This results in a cloud fraction maximum that is more pronounced and more spread out, with a peak at a higher level; however, above the maximum, cloud fraction also decreases more rapidly with height (Fig. 10a). Thus, in this model, convective warming stabilizes the lowest atmospheric layers (Fig. 10c), explaining the shallower turbulent mixing when convection is switch on (Fig. 10d). This reduces the turbulent transport of humidity below 900 hPa, leads to shallower low clouds, and decreases the low-cloud fraction.

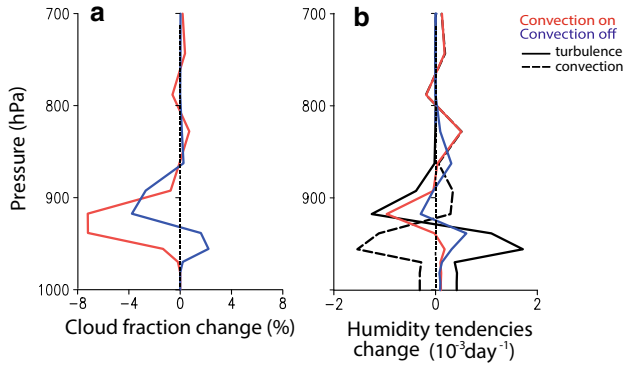

Fig. 11 Changes of **a** cloud fraction and **b** specific humidity tendencies under a 2-K warming in IPSL-CM5A SCM with (*red*) and without (*blue*) a convection scheme. Total (turbulent plus convective) tendencies from experiments with convection (*red lines*) are separated into tendencies owing to parameterized turbulence (*black solid lines*) and into tendencies owing to parameterized convection (*black dashed lines*) in **b**

If we compare the present with a warmer climate (prescribed SST increased by 2 K), the low clouds deepen ($\Delta\gamma < 0$) in the simulation with convection, and their cloud fraction decreases substantially (Fig. 11a). In the simulation without convection, by contrast, the low clouds become shallower ($\Delta\gamma > 0$), and their cloud fraction decreases only weakly. The shallowing arises because the turbulent mixing in the PBL weakens when convection is switched off. This may seem to stand in contrast to the negative low-cloud feedback that was posited to be induced by increased surface fluxes and turbulent moistening as the climate warms (Kawai 2012; Zhang et al. 2013); however, as we have seen before, the static stability increases and the sensible heat fluxes generally weaken as the climate warms (Fig. 3b), so a weakening of turbulent mixing is plausible. The deepening arises as convection increasingly ventilates the PBL by transporting more moisture from the surface to the free troposphere, which favors mid-level clouds at the expense of PBL clouds. The net result of these opposing effects gives the overall change in low-cloud fraction: the strong decrease with convection, and the much weaker decrease without convection in the IPSL-CM5A SCM.

The convective drying index ε_c and changes in the implied total humidity diffusivities K_i for these SCM experiments confirm these results. Without the convection parameterization, the shallowing of low clouds under warming is associated with a reduction of total moisture mixing (Fig. 8a, circle). With the convection parameterization, convective drying is strong, and its strengthening under warming overcompensates strengthened turbulent moistening, leading to an increased total moisture mixing and the deepening of low clouds (triangle in Figs. 7b, 8a and 11).

6 Discussion and conclusions

Our analyses have shown that in state-of-the-art climate models, greater shallowness of low clouds in weak-subsidence regimes is associated with greater climate sensitivity. How shallow low clouds are in a given model is controlled by the competition between parameterized convective drying and turbulent moistening, which together account for the total parameterized moisture mixing in a model. In the present-day climate, models with stronger convective drying tend to have shallower low clouds. As the climate warms, low clouds in a model may become shallower or deeper, depending on the change of total moisture mixing by parameterized convection and turbulence.

Robust mechanisms explain the opposing effects of parameterized convection and turbulence. As the surface warms, evaporation intensifies, and the atmospheric temperature and specific humidity increase. This has two consequences for changes in moisture mixing. First, because the relative humidity near the surface is energetically constrained to change little, the magnitude of the vertical specific humidity gradient increases, and the convective moisture mixing is expected to strengthen (e.g., if the convective mass flux changes less in fractional terms than the specific humidity). This suggests a positive low-cloud feedback, in which convective PBL drying leads to reductions in cloud cover (e.g., Zhang et al. 2013). Second, the lower atmosphere stabilizes and sensible heat fluxes weaken, which suggests a weakening of turbulent diffusivity. This may result in a shallowing of total moisture mixing in the boundary layer. The relative importance of these two mechanisms controls the change of shallowness and the response in low-cloud fraction in climate models, as summarized in Fig. 12.

By contrast to surface warming, the direct effect of CO_2 concentration increases leads to shallower low clouds in climate models (Kamae and Watanabe 2012, 2013). The shallowing arises because convective mixing does not strengthen appreciably in response to CO_2 concentration increases, so that low clouds react only to the weakened turbulent mixing, similar to our experiments in which convection was switched off.

These results highlight that (1) the climatological shallowness of low clouds is an indicator of the relative importance of parameterized convective and turbulent mixing in climate models, and its variations across models account for about half of the spread (intermodel standard deviation) in their climate sensitivities; and (2) low-cloud shallowing or deepening (suggesting different strength of the low-cloud feedback) can arise depending on the relative importance of parameterized convective and turbulent mixing. Observations suggest an intermediate shallowness index

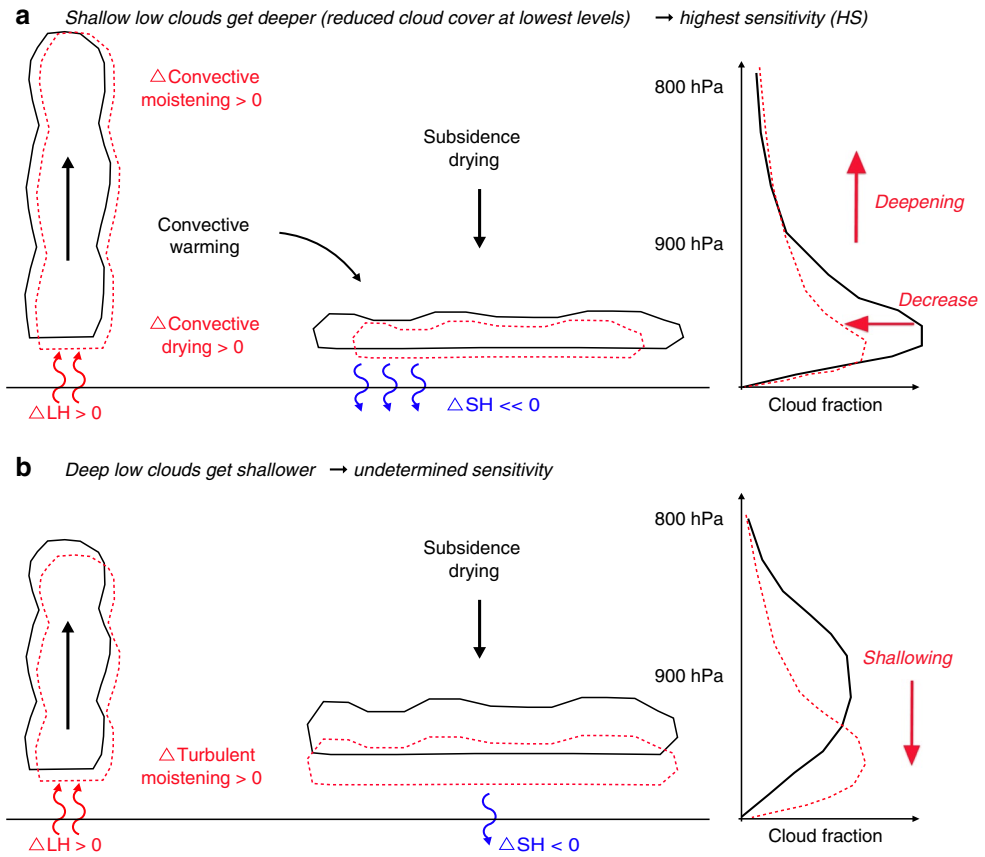

Fig. 12 Schematic of the physical mechanisms in climate models that control the tropical low-cloud distribution for the present (*black lines*) and a warmer climate (*red* and *blue* referring to positive and negative changes). Models simulating deepening (**a**) and shallowing (**b**) of low clouds under warming are separated. An equilibrium between turbulent and convective moistening controls where low clouds form. Convective warming (in addition to large-scale fluxes) stabilizes the lower troposphere and contributes to shallower low clouds. As the climate warms, two mechanisms act: (1) enhanced evaporation and strengthened specific humidity gradients strengthen convective mixing; (2) the lower atmosphere stabilizes, leading to weakened turbulent mixing. Models simulating low-cloud shallowing (**b**) are more influenced by the weakened turbulent mixing; models simulating low-cloud deepening (**a**) are more influenced by strengthened convective mixing

of around $\gamma \approx 45 \pm 4\,\%$. Models that have a shallowness γ broadly consistent with this value have climate sensitivities between 2.4 and 4.6 K.

The climatological shallowness of low clouds is intrinsically linked to the intensity of lower-tropospheric mixing, which has previously been identified as a control on models' climate sensitivity (Sherwood et al. 2014). Sherwood et al. showed that higher climate sensitivity and a stronger positive low-cloud feedback in climate models arise when convective mixing is stronger. They suggested that models with stronger convective mixing dry the PBL more efficiently as the surface warms, leading to a stronger reduction in low-cloud cover and hence higher climate sensitivity. Our results show that this mechanism occurs in every model but controls the low-cloud response only in about half of the CMIP5 models (those with $\Delta\gamma < 0$). The other half is dominated by low-cloud shallowing caused by weakened turbulent moistening. The level of compensation between the two processes is highly variable among models, accounting for part of the spread of low-cloud responses and climate sensitivities seen in global warming simulations.

This study suggests that model developments that improve how low clouds are distributed vertically may increase the reliability of how the low-cloud response to climate change is simulated. These developments may be informed by comparisons of the climatology and temporal variability of the vertical structure of low clouds between models and observations, along the lines of what was done by Nuijens et al. (2015). Such analyses may help reduce the spread of climate sensitivity in the future. Reliable verification of the vertical structure of low clouds in models will also require a continuous effort to monitor three-dimensional cloud structures observationally (Winker et al. 2010; EarthCARE Mission Advisory Group 2006).

Acknowledgments This work was supported by the Department of Energy's Regional and Global Climate Modeling Program under the project "Identifying Robust Cloud Feedbacks in Observations and Model". We thank Bjorn Stevens, Louise Nuijens, Steve Klein and Peter Caldwell for useful discussions on this topic and two anonymous reviewers for their insightful comments on the manuscript. We acknowledge the World Climate Research Programme's Working Group on Coupled Modelling, which is responsible for CMIP, and we thank the climate modeling groups (listed in Table 1) for producing and making available their model output.

References

Anderson J et al (2004) The new GFDL global atmosphere and land model AM2–LM2: evaluation with prescribed SST simulations. J Clim 17:4641–4673

Arakawa A, Schubert WH (1974) Interaction of a cumulus cloud ensemble with the large-scale environment, part I. J Atmos Sci 31:674–701

Betts AK (1986) A new convective adjustment scheme. Part I: observational and theoretical basis. Q J R Meteorol Soc 112:677–691

Blackadar AK (1962) The vertical distribution of wind and turbulent exchange in a neutral atmosphere. J Geophys Res 67:3095–3102

Boer G (1993) Climate change and the regulation of the surface moisture and energy budgets. Clim Dyn 8:225–239

Bony S, Dufresne J-L (2005) Marine boundary layer clouds at the heart of tropical cloud feedback uncertainties in climate models. Geophys Res Lett 32:L20806

Bony S, Dufresne J-L, LeTreut H, Morcrette J-J, Senior C (2004) On dynamic and thermodynamic components of cloud changes. Clim Dyn 22:71–86

Bony S, Emanuel KA (2001) A parameterization of the cloudiness associated with cumulus convection; evaluation using TOGA COARE data. J Atmos Sci 58:3158–3183

Bony S et al (2006) How well do we understand and evaluate climate change feedback processes? J Clim 19:3445–3482

Bony S et al (2013) Carbon dioxide and climate: perspectives on a scientific assessment. Climate Science for Serving Society. Springer, Berlin, pp 391–413

Bretherton C, Ferrari R, Legg S (2004) Climate process teams: a new approach to improving climate models. US CLIVAR Var 2:1–6

Bretherton CS, Blossey PN, Jones CR (2013) Mechanisms of marine low cloud sensitivity to idealized climate perturbations: a single-LES exploration extending the CGILS cases. J Adv Model Earth Syst 5:316–337

Brient F, Bony S (2012) How may low-cloud radiative properties simulated in the current climate influence low-cloud feedbacks under global warming? Geophys Res Lett 39:L20807. doi:10.1029/2012GL053265

Brient F, Bony S (2013) Interpretation of the positive low-cloud feedback predicted by a climate model under global warming. Clim Dyn 40:2415–2431

Brinkop S, Roeckner E (1995) Sensitivity of a general circulation model to parameterizations of cloud-turbulence interactions in the atmospheric boundary layer. Tellus A 47:197–220

Cess R et al (1996) Cloud feedback in atmospheric general circulation models: an update. J Geophys Res 101:12 791–12 794

Cess RD et al (1990) Intercomparison and interpretation of climate feedback processes in 19 atmospheric general circulation models. J Geophys Res 95(601):216

Charney JG et al (1979) Carbon dioxide and climate: a scientific assessment. National Academy of Sciences, Washington

Chepfer H, Bony S, Winker D, Cesana G, Dufresne J, Minnis P, Stubenrauch C, Zeng S (2010) The GCM-oriented CALIPSO cloud product (CALIPSO-GOCCP). J Geophys Res 115

Chikira M, Sugiyama M (2010) A cumulus parameterization with state-dependent entrainment rate. Part I: description and sensitivity to temperature and humidity profiles. J Atmos Sci 67:2171–2193

Cuijpers J, Bechtold P (1995) A simple parameterization of cloud water related variables for use in boundary layer models. J Atmos Sci 52:2486–2490

Dee D et al (2011) The ERA-interim reanalysis: configuration and performance of the data assimilation system. Q J R Meteorol Soc 137:553–597

Del Genio A, Yao M (1993) Efficient cumulus parameterization for long-term climate studies: the GISS scheme. The representation of cumulus convection in numerical models. Meteorol Monogr 46:181–184

Del Genio A, Yao M, Kovari W (1996) A prognostic cloud water parameterization for global climate models. J Clim 9:270–304

Donner LJ et al (2011) The dynamical core, physical parameterizations, and basic simulation characteristics of the atmospheric component AM3 of the GFDL global coupled model CM3. J Clim 24:3484–3519

Dufresne J-L, Bony S (2008) An assessment of the primary sources of spread of global warming estimates from coupled atmosphere-ocean models. J Clim 21:5135–5144

EarthCARE Mission Advisory Group (2006) Earthcare mission requirement document. Technical report, ESA. http://esamultimedia.esa.int/docs/EarthObservation/EarthCARE_MRD_v5.pdf

Emanuel K (1991) A scheme for representing cumulus convection in large-scale models. J Atmos Sci 48:2313–2329

Emanuel K (1993) A cumulus representation based on the episodic mixing model: the importance of mixing and microphysics in predicting humidity. AMS Meteorol Monogr 24:185–192

Emori S, Nozawa T, Numaguti A, Uno I (2001) Importance of cumulus parameterization for precipitation simulation over East Asia in June. J Meteorol Soc Jpn 79:939–947

Forster PM, Andrews T, Good P, Gregory JM, Jackson LS, Zelinka M (2013) Evaluating adjusted forcing and model spread for historical and future scenarios in the CMIP5 generation of climate models. J Geophys Res 118:1139–1150

Gettelman A, Kay J, Shell K (2012) The evolution of climate sensitivity and climate feedbacks in the community atmosphere model. J Clim 25:1453–1469

Gregory D, Rowntree P (1990) A mass flux convection scheme with representation of cloud ensemble characteristics and stability-dependent closure. Mon Weather Rev 118:1483–1506

Gregory J, Webb M (2008) Tropospheric adjustment induces a cloud component in CO_2 forcing. J Clim 21:58–71

Hack JJ (1994) Parameterization of moist convection in the National Center for Atmospheric Research community climate model (CCM2). J Geophys Res 99:5551–5568

Hartmann DL, Larson K (2002) An important constraint on tropical cloud-climate feedback. Geophys Res Lett 29:1951–1954

Held IM (1982) On the height of the tropopause and the static stability of the troposphere. J Atmos Sci 39:412–417

Held IM, Soden BJ (2006) Robust responses of the hydrological cycle to global warming. J Clim 19:5686–5699

Hourdin F et al (2013) LMDZ5B: the atmospheric component of the IPSL climate model with revisited parameterizations for clouds and convection. Clim Dyn 40:2193–2222

Jam A, Hourdin F, Rio C, Couvreux F (2013) Resolved versus parametrized boundary-layer plumes. Part III: derivation of a statistical scheme for cumulus clouds. Boundary Layer Meteorol 147:421–441

Kamae Y, Watanabe M (2012) On the robustness of tropospheric adjustment in CMIP5 models. Geophys Res Lett 39:L23808. doi:10.1029/2012GL054275

Kamae Y, Watanabe M (2013) Tropospheric adjustment to increasing CO_2: its timescale and the role of land-sea contrast. Clim Dyn 41:3007–3024

Kawai H (2012) Examples of mechanisms for negative cloud feedback of stratocumulus and stratus in cloud parameterizations. Sci Online Lett Atmos 8:150–154

Laval K, Sadourny R, Serafini Y (1981) Land surface processes in a simplified general circulation model. Geophys Astrophys Fluid Dyn 17:129–150

Le Treut H, Li Z (1991) Sensitivity of an atmospheric general circulation model to prescribed sst changes: feedback effects associated with the simulation of cloud optical properties. Clim Dyn 5:175–187

Lock A, Brown A, Bush M, Martin G, Smith R (2000) A new boundary layer mixing scheme. Part I: scheme description and single-column model tests. Mon Weather Rev 128:3187–3199

Louis J (1979) A parametric model of vertical eddy fluxes in the atmosphere. Bound Layer Meteorol 17:187–202

McFarlane NA, Boer G, Blanchet J, Lazare M (1992) The Canadian Climate Centre second-generation general circulation model and its equilibrium climate. J Clim 5:1013–1044

Mellor GL, Yamada T (1974) A hierarchy of turbulence closure models for planetary boundary layers. J Atmos Sci 31:1791–1806

Mellor GL, Yamada T (1982) Development of a turbulence closure model for geophysical fluid problems. Rev Geophys 20:851–875

Mitchell JF, Wilson C, Cunnington W (1987) On CO_2 climate sensitivity and model dependence of results. Q J R Meteorol Soc 113:293–322

Moeng C-H, Sullivan PP (1994) A comparison of shear-and buoyancy-driven planetary boundary layer flows. J Atmos Sci 51:999–1022

Moorthi S, Suarez MJ (1992) Relaxed Arakawa–Schubert—a parameterization of moist convection for general circulation models. Mon Weather Rev 120:978–1002

Neale R, Richter J, Conley A, Lauritzen P, Gettelman A, Williamson D (2010) Description of the NCAR Community Atmosphere Model (CAM 4.0). National Center for Atmospheric Research Technical Report

Nuijens L, Medeiros B, Sandu I, Ahlgrimm M (2015) The behavior of trade-wind cloudiness in observations and models: The major cloud components and their variability. J Adv Model Earth Syst 7:600–616.doi:10.1002/2014MS000390

O'Gorman PA, Schneider T (2008) The hydrological cycle over a wide range of climates simulated with an idealized GCM. J Clim 21:3815–3832

Pan D-M, Randall DD (1998) A cumulus parameterization with a prognostic closure. Q J R Meteorol Soc 124:949–981

Pierrehumbert RT (2002) The hydrologic cycle in deep-time climate problems. Nature 419:191–198

Rieck M, Nuijens L, Stevens B (2012) Marine boundary layer cloud feedbacks in a constant relative humidity atmosphere. J Atmos Sci 69:2538–2550

Schneider T, O'Gorman PA, Levine XJ (2010) Water vapor and the dynamics of climate changes. Rev Geophys 48:RG3001. doi:10.1029/2009RG000302

Sherwood SC, Bony S, Dufresne J-L (2014) Spread in model climate sensitivity traced to atmospheric convective mixing. Nature 505:37–42

Singh MS, O'Gorman PA (2012) Upward shift of the atmospheric general circulation under global warming: theory and simulations. J Clim 25:8259–8276

Slingo J (1987) The development and verification of a cloud prediction scheme for the ECMWF model. Q J R Meteorol Soc 113:899–927

Smith R (1990) A scheme for predicting layer clouds and their water content in a general circulation model. Q J R Meteorol Soc 116:435–460

Soden B, Broccoli AJ, Hemler RS (2004) On the use of cloud forcing to estimate cloud feedback. J Clim 17:3661–3665

Stevens B et al (2013) Atmospheric component of the mpi-m earth system model: ECHAM6. J Adv Model Earth Syst 5:146–172

Sundqvist H, Berge E, Kristjansson J (1989) Condensation and cloud parameterization studies with a mesoscale numerical weather prediction model. Mon Weather Rev 117:1641–1657

Taylor KE, Stouffer RJ, Meehl GA (2012) An overview of CMIP5 and the experiment design. Bull Am Meteorol Soc 93:485–498

Thuburn J, Craig GC (1997) GCM tests of theories for the height of the tropopause. J Atmos Sci 54:869–882

Tiedtke M (1989) A comprehensive mass flux scheme for cumulus parameterization in large-scale models. Mon Weather Rev 117:1779–1800

Tiedtke M (1993) Representation of clouds in large-scale models. Mon Weather Rev 121:3040–3061

Tomassini L, Voigt A, Stevens B (2014) On the connection between tropical circulation, convective mixing, and climate sensitivity. Q J R Meteorol Soc 141:1404–1416

Vial J, Dufresne J-L, Bony S (2013) On the interpretation of inter-model spread in CMIP5 climate sensitivity estimates. Clim Dyn 41:3339–3362

Volodin E, Dianskii N (2004) El Nino in a coupled ocean-atmosphere general circulation model. Russ Meteorol Hydrol 12:1

von Salzen K, McFarlane N, Lazare M (2005) The role of shallow convection in the water and energy cycles of the atmosphere. Clim Dyn 25:671–688

von Salzen K et al (2013) The Canadian fourth generation atmospheric global climate model (CanAM4). Part I: representation of physical processes. Atmos Ocean 51:104–125

Watanabe M, Emori S, Satoh M, Miura H (2009) A PDF-based hybrid prognostic cloud scheme for general circulation models. Clim Dyn 33:795–816

Watanabe M et al (2010) Improved climate simulation by MIROC5: mean states, variability, and climate sensitivity. J Clim 23:6312–6335

Watanabe M et al (2012) Using a multi-physics ensemble for exploring diversity in cloud-shortwave feedback in GCMs. J Clim 25:5416–5431

Webb M et al (2006) On the contribution of local feedback mechanisms to the range of climate sensitivity in two GCM ensembles. Clim Dyn 27:17–38

Webb MJ, Lock AP (2013) Coupling between subtropical cloud feedback and the local hydrological cycle in a climate model. Clim Dyn 41:1923–1939

Winker D et al (2010) The CALIPSO mission: a global 3D view of aerosols and clouds. Bull Am Meteorol Soc 91:1211–1229

Wu T et al (2010) The Beijing Climate Center atmospheric general circulation model: description and its performance for the present-day climate. Clim Dyn 34:123–147

Wyant MC, Bretherton CS, Blossey PN (2009) Subtropical low cloud response to a warmer climate in a superparameterized climate model. Part I: regime sorting and physical mechanisms. J Adv Model Earth Syst 1:1–11

Yamada T (1983) Simulations of nocturnal drainage flows by a q^2l turbulence closure model. J Atmos Sci 40:91–106

Yao M-S, Cheng Y (2012) Cloud simulations in response to turbulence parameterizations in the GISS Model E GCM. J Clim 25:4963–4974

Yukimoto S et al (2011) Meteorological Research Institute Earth System Model Version 1 (MRI-ESM1)—model description. Technical Reports of the Meteorological Research Institute 1

Zhang GJ, McFarlane NA (1995) Sensitivity of climate simulations to the parameterization of cumulus convection in the Canadian Climate Centre general circulation model. Atmos Ocean 33:407–446

Zhang GJ, Mu M (2005) Effects of modifications to the Zhang-McFarlane convection parameterization on the simulation of the tropical precipitation in the National Center for Atmospheric Research Community Climate Model, version 3. J Geophys Res 110(D09):109

Zhang MH et al (2013) CGILS: first results from an international project to understand the physical mechanisms of low cloud feedbacks in general circulation models. J Adv Model Earth Syst 5:826–842